Observation of Coherent Surface Optical Phonon Oscillations by Time-Resolved Surface Second-Harmonic Generation

Y. M. Chang, L. Xu, and H. W. K. Tom
Department of Physics, University of California, Riverside, California 92521
(Received 12 November 1996)

We demonstrate a new time-domain surface phonon spectroscopy. We excite coherent surface optical phonons with an ultrashort laser pulse and probe the free-induction decay with time-resolved surface second-harmonic generation. For both clean GaAs (110) and (100) surfaces, the signals are remarkably large due to the highly localized electron-phonon interaction at the surface and the intrinsic surface sensitivity of second-harmonic generation. This work suggests that coherent oscillations of surface optical phonons may be used as probes of electron-phonon interactions at surfaces and to control or drive nonthermal surface chemical reactions. [S0031-9007(97)03165-7]

PACS numbers: 78.66.–w, 42.50.Md, 68.35.Ja, 78.47.+p

Advances in femtosecond laser technology have made it possible to excite, probe, and to even "control" coherent excitations of electronic and vibrational states of atoms, molecules, and solids. Kurz and co-workers [1,2] and Ippen and co-workers [3,4] have demonstrated the excitation of coherent longitudinal optical (LO) phonons in *bulk* semiconductors, semimetals, and insulators using femtosecond laser pulses and their detection by time-resolved linear reflectivity. Here we demonstrate that we can excite coherent optical phonons on *surfaces* using femtosecond laser pulses and probe those modes by time-resolving the second-harmonic generation (TRSHG) from the surface.

This work presents a new technique for studying surface phonons [5]. Currently the most widely used techniques are He atom scattering (HAS) and high-resolution electron-energy-loss spectroscopy (HREELS). Both are surface sensitive and can probe wave vectors throughout the entire surface Brillouin zone. HAS [6] and HREELS [7] studies of the clean 1×1 relaxed GaAs (110) surface have been reported. Raman scattering and resonance Raman scattering have been used to study phonons localized at the Sb/GaAs(110) interface [8,9], but not the clean surface. Like Raman scattering, our new surface phonon spectroscopy technique is all-optical and can only probe the phonons at the center of the Brillouin zone (surface $\overline{\Gamma}$ point). However, it has the advantages of surface SHG: it is surface sensitive and can be used at buried interfaces or interfaces with dense gases. We observed six optical phonon modes on the 1×1 relaxed GaAs (110) surface which agree quantitatively with recent calculations [10,11]. Even modes not easily observed in HREELS [7] are observed. Our results on various GaAs (100) reconstructed surfaces will be published elsewhere but show a large number of modes and comparable signal amplitudes.

Experiments were carried out under ultrahigh vacuum conditions ($<2 \times 10^{-10}$ torr). The 1×1 relaxed GaAs (110) surface was prepared by cycles of argon ion sputtering at 500 eV and thermal annealing at 550 °C until Auger electron spectroscopy showed $<1\%$ contamination and low energy electron diffraction showed a sharp (1×1) pattern. Optical experiments were performed using 850 nm, 35 fs laser pulses from a Ti:sapphire Kerr-lens mode-locked laser oscillator with $\sim$80 MHz repetition rate. The weak probe beam was derived from the pump with a beam splitter. The pump beam was passed through a delay line. Pump and probe pulses overlapped spatially in a Gaussian spot on the sample at 45° angle of incidence with a $\sim$3° angular separation perpendicular to the plane of incidence. The p-polarized SH generated by the p-polarized probe beam ($p_{\text{in}} - p_{\text{out}}$) was passed through a color filter, polarizer, and interference filter and detected with a thermoelectric-cooled photomultiplier tube. The change in probe SHG due to the pump was detected using a lock-in amplifier synchronized to the chopping rate of the pump.

In Fig. 1 we show the differential (pump-induced) SHG as a function of pump-probe time delay. The zero of time delay is calibrated by detecting the pump-probe cross-correlation SHG from the sample. The rapid rise during the pump pulse is due to the injection of carriers. The TRSHG decays on the $\sim$300 fs time scale due to carrier screening of the depletion field and on the $\sim$4 ps time

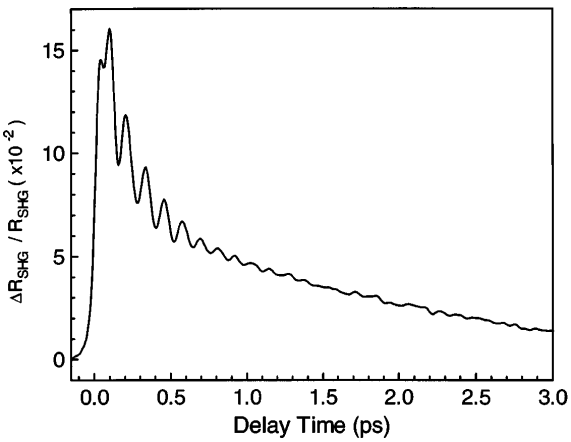

FIG. 1. Differential p_{in}-p_{out} TRSHG for GaAs (110) (1×1) surface. [001] in plane of incidence, pump is s polarized.

scale due to carrier recombination and diffusion. Full analysis of these features will appear elsewhere but is similar to the behavior observed and analyzed by Kurz and co-workers [2]. Here we concentrate on the small oscillations which are ~15% of the maximum differential amplitude and about 2% of the total SHG signal. These oscillations are due to excitation of coherent optical phonons at the surface or near suface bulk. In contrast, coherent bulk LO phonons generate a 10^{-4} fractional change in time-resolved linear reflectivity [1].

In Fig. 2(a) we show the oscillatory part of the time-resolved SHG data for four excitation geometries where the sample is oriented with either the crystalline $x = [001]$ or $y = [1\bar{1}0]$ axes parallel to the plane of incidence, and either s or p polarized pump pulses. The oscillatory part is obtained from data as in Fig. 1 by cutting off the first 150 fs of time delay and Fourier filtering the slow decay. These oscillations decay in time as one would expect for free-induction decay of a coherent excitation. Mode beating is apparent. In Fig. 2(b) we show the Fourier power spectra of the data in Fig. 2(a) using a $\sin(t)/t$ apodizing function to minimize artifacts due to the finite extent of the time-domain data.

The peak at 8.76 THz is observed in all traces and is due to the bulk LO phonon in the underlying bulk region. It is the same mode observed in time-resolved linear reflectivity [1]. The mode is driven by rapid carrier-induced screening of the depletion field which extends only ~135 Å deep for this highly doped sample (n-type 3×10^{18} Si/cm^3). Detailed numerical simulations following those in Ref. [2] indicate the peak LO displacement is ~0.01 Å located about 30 Å from the surface plane. The excitation extends ~50 Å full width half maximum in depth. The injected carrier density is kept low enough to prevent the appearance of the bulk LO phonon-electron plasma coupled mode which is observed in the range 7.3–7.7 THz for higher excitation levels [5].

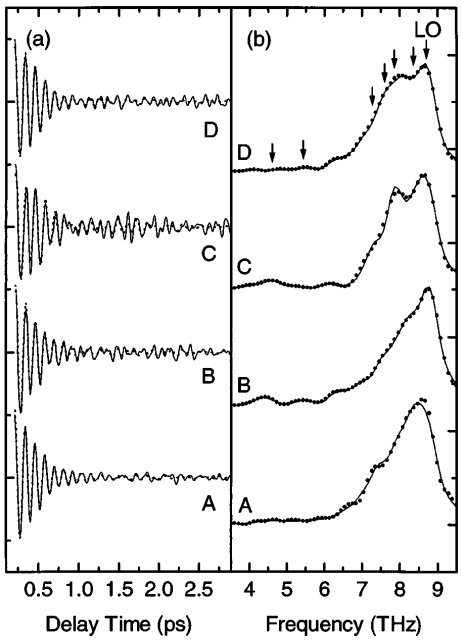

FIG. 2. (a) Oscillatory part and (b) Fourier power spectra of differential p_{in}-p_{out} TRSHG for four geometries. *A*: [001] ∥ plane, *s*-pol. pump. *B*: [001] ∥ plane, *p*-pol. pump. *C*: [1$\bar{1}$0] ∥ plane, *s*-pol. pump. *D*: [110] ∥ plane, *p*-pol. pump. Data in solid lines and results of curve fitting in dotted lines. Arrows show phonon frequencies obtained from fit.

All the other modes (1–6 in Table I) are due to surface phonon modes localized to the topmost three Ga-As layers. The mode features (center frequency and linewidth) depend strongly on the quality of the surface reconstruction as evidenced by LEED, are different for the GaAs (110) and (100) surface, broaden and disappear when the topmost three layers are disordered by argon ion sputtering (dosage corresponding to removal of 1 GaAs layer), and shift, broaden, and disappear during controlled room temperature oxidation (O_2 exposure with lit filament).

We now consider the data in detail. The SH electric field is driven by the nonlinear polarization $\vec{P}(2\omega) = \vec{\chi}^{(2)}(2\omega) : \vec{E}(\omega)\vec{E}(\omega)$, where $\overleftrightarrow{\chi}^{(2)}(2\omega)$ is the SH susceptibility tensor and $\vec{E}(\omega)$ is the fundamental frequency electric field. $\overleftrightarrow{\chi}^{(2)}(2\omega)$ may be expanded in the phonon displacement:

$$\overleftrightarrow{\chi}^{(2)}(2\omega) = \overleftrightarrow{\chi}^{(2)}(2\omega)|_0 + \sum_n [\partial \overleftrightarrow{\chi}^{(2)}(2\omega)/\partial \hat{u}_n]|_0 U_n , \quad (1)$$

where U_n is the amplitude of the nth phonon mode and the differential second-order polarizability is taken with respect to $\hat{u}_n$ the normalized phonon polarization vector and is evaluated at the equilibrium point. The index n includes the phonon branch and wave vector. In the harmonic approximation, each mode obeys

$$\ddot{U}_n + \dot{U}_n/T_n + (2\pi\nu_n)^2 U_n = F_n/\mu_n ,$$

where T_n, ν_n, F_n, and μ_n are the mode's dephasing time, resonant frequency, external force, and effective mass.

In this experiment, we use a laser beam with Gaussian waist around 10 μm and thus can only excite surface modes with wave vector $q_\parallel < 1\ \mu\text{m}^{-1}$. For such small values of $q_\parallel$ we can ignore dispersion. In thermal equilibrium the lack of coherence between the modes of different surface wave vector washes out any contribution to Eq. (1) from each mode branch. However, a coherent force applied to the system can drive modes of different $q_\parallel$ in phase and thus provide a modulation detectable through Eq. (1). In our experiment, the time duration of F_n is short compared to the oscillation period and dephasing time. After 100 fs delay time, the excited modes of the same branch oscillate in phase at the same frequency—as if a single $q_\parallel = 0$ mode were excited.

Physically, there is only one set of normal modes for this surface, so we fit all four curves in Fig. 2 to the function

$$S(t) = \sum_n A_n \cos(2\pi\nu_n t + \varphi_n) e^{-t/T_n},$$

TABLE I. Fit results and symmetry of surface phonons observed on GaAs (110) (1 × 1) and previous HREELS and theoretical values.

n	ν_n (THz)	T_n (fs)	Sym.	Expt. [7]	Theory [10]	Theory [11]
	8.76 ± 0.01	740 ± 80		8.76	bulk LO	
1	8.35 ± 0.07	800 ± 30	A'		8.36	
2	7.85 ± 0.01	470 ± 10	A'		7.86	
3	7.58 ± 0.01	720 ± 50	A'		7.56	
4	7.29 ± 0.03	550 ± 30	A'		7.37	
5	5.41 ± 0.04	600 ± 150	A'/A''	5.5 ± 0.25	5.80	5.32
						5.56
6	4.57 ± 0.05	790 ± 140	A'	3.9 ± 0.4	3.98	3.94

where ν_n and T_n are the same for the four curves but the amplitude, A_n, and initial temporal phase, φ_n, are allowed to be different because of the different elements of $\partial\vec{\chi}^{(2)}/\partial\hat{u}_n$. The SH intensity is proportional to $|\chi|^2$. Because the oscillatory part is only 2% of the total signal, it is only 1% of $|\chi|$, and we ignore the square of the oscillatory part. The fitting process required iterative fitting between the time data (sensitive to A_n and T_n) and the complex Fourier transform (sensitive to ν_n and φ_n). The dotted lines in Fig. 2 are the fits and the ν_n values are indicated with arrows. The apparent maxima in the Fourier spectra are shifted from ν_n by interference with neighboring modes. Small features such as that at 9.3 THz are artifacts from the apodization. The fit values are listed in Table I. The fits to the data are excellent and the constraint of fitting the four curves simultaneously gives us an error bar $<\pm 0.1$ THz despite the large number of free parameters. Our resolution is better than in HREELS (± 1 meV $= 0.25$ THz).

In Table I we list mode frequencies from HREELS data [7], an *ab initio* calculation [10], and a tight-binding total-energy minimization model calculation [11]. Our observed mode at 8.35 THz is predicted in the *ab initio* calculation to be dominated by the opposing motion of the topmost Ga and second layer As perpendicular to the chains. This mode is the TO branch of the LO-TO split surface optical phonon mode in analogy to the bulk LO and TO modes. The Fuchs-Kliewer mode is the LO branch.

The Fuchs-Kliewer optical surface phonon mode at 8.71 THz (35.8 meV) dominates HREELS [7,12] but is NOT observed in this work. The Fuchs-Kliewer mode varies spatially as $\exp(iq_{\|}x - q_{\|}z)$ [13]. Since we only excite modes with $q_{\|} < 1\ \mu\text{m}^{-1}$, these modes extend $>1\ \mu$m into the bulk and would not be detectable by SHG which is only sensitive to the top ~200 Å (effective coherence length) of the bulk. In HREELS the *minimum* detectable $q_{\|}$ limits depth to <200 Å.

We observe 3 modes in the range of 7–8 THz which are predicted from the *ab initio* calculation to have peak displacement amplitude in layers two and three and to have opposing Ga-As motion mostly parallel to the plane. The agreement with theory is extraordinary but consistent with 3 modes in a narrow frequency range. These 3 modes are not observed in HREELS—perhaps because they are largely polarized in the plane.

The mode at 5.41 THz matches the value measured in HREELS but is well below the value 5.80 THz predicted in the *ab initio* calculation for the motion of the topmost As atom perpendicular to the chain. Our value agrees better with Ref. [11] in which there are two shear modes of the topmost Ga and As atoms parallel ($1A''$ at 5.32 THz) and perpendicular ($3A'$ at 5.56 THz) to the zigzag chain. Interestingly, the only mode that we detected that could have A'' symmetry is the 5.41 THz mode.

We also measure a mode at 4.57 THz which is just above the error bar of the HREELS measurement. The *ab initio* calculation predicts a mode at 4 THz dominated by motion of the topmost Ga atom perpendicular to the chain. The tight-binding calculation predicts a bond-length preserving rotation of the topmost Ga and As atoms in the direction perpendicular to the chain, also at 4 THz. We may have better resolution than the HREELS measurement or we may be detecting an additional mode which is dominated by in plane motion and thus not easily detected in HREELS.

The selection rule for detecting modes with SHG is that the differential second-order polarizability, which is a third rank tensor, be nonzero. The mode must be hyper-Raman active. For comparison, in specular scattering, HREELS is most sensitive to modes which are ir active perpendicular to the surface. This may be an additional reason why four of the six modes in the table are not detected in HREELS. The symmetry of the hyper-Raman tensor allows us to deduce the symmetry of the mode by measuring the SH in different excitation geometries. The symmetry of the (110) surface is m and modes are either A' (symmetric) or A'' (antisymmetric) upon mirror in the x-z plane. Only A' modes can be detected by SH when the $x = [100]$ axis is in the plane of incidence. Both A' and A'' modes can be detected when the $y = [1\bar{1}0]$ axis is in the plane of incidence. The appearance of a mode only in this geometry is necessary but not sufficient to identify it as A''. The mode identifications are noted in Table I.

The force F_n that drives the coherent optical phonons can be due to four general mechanisms. The first two involve rapid increases in carrier density leaving the atoms

suddenly in vibrationally excited positions with respect to new equilibrium positions. Ippen and co-workers have called the first of these mechanisms displacive excitation of coherent phonons (DECP) [4]. Only fully symmetric A' modes can be excited. A second mechanism applies to semiconductors with built-in surface electric fields which induce static LO phonon displacements. When laser-injected carriers rapidly screen the field, the lattice is suddenly free to oscillate about the field free lattice positions. This is the dominant mechanism for exciting the bulk LO phonons in the depletion region of GaAs [2]. A third driving mechanism is stimulated Raman excitation (SRE). The force is $F_n = \frac{1}{2}\varepsilon_0[\partial\boldsymbol{\alpha}^{(1)}/\partial\hat{u}_n]_0 : \boldsymbol{EE}^*$, where the differential linear polarizability per unit cell is evaluated at the equilibrium point and is related to the Raman scattering cross section. Since $\boldsymbol{EE}^*$ is proportional to the laser intensity, any Raman active mode with vibrational period less than the laser pulse width can be excited. This mechanism dominates coherent vibrational excitation of molecules and molecular crystals [14]. The fourth driving mechanism is the Franck-Condon effect for molecules or the generalized Menzel-Gomer-Redhead (MGR) type mechanism for surfaces [15]. On surfaces, electronic lifetimes are <100 fs and thus short compared to vibrational periods. The atoms accelerate while briefly in the electronically excited state and return to the ground electronic state vibrationally excited. Both SRE and MGR have Raman selection rules. SRE is a coherent process and MGR involves excited population. All 4 mechanisms require the laser pulse to be short.

Examination of the *A*-*B* and *C*-*D* pairs of data in Fig. 2(b) shows that when the pump laser polarization is changed the SH signal changes for all modes. Only SRE and MGR mechanisms can depend on the pump polarization—DECP and "field screening" depend only on the number of injected carriers. Thus all 6 local surface modes we detected were driven by SRE or MGR mechanisms.

The detected signal amplitude is proportional to the driving term, which for both SRE and MGR scales as the $\partial\boldsymbol{\alpha}^{(1)}/\partial\hat{u}$, and to the sensitivity of SH detection via $\partial\boldsymbol{\alpha}^{(2)}/\partial\hat{u}$. Both tensors are unknown, however, the SH oscillation signals for the coherent surface phonons are extraordinarily large—the same order of magnitude as that for the bulk LO phonons. We calculated the bulk LO phonon amplitude to be 0.01 Å over $\sim$50 Å depth. The surface phonons must be localized to $\sim$5 Å—10 times fewer atomic layers. Moreover, the Raman cross section per layer for the bulk is 40 times too small to produce the same amplitude in the bulk. The product of $\partial\boldsymbol{\alpha}^{(1)}/\partial\hat{u}$ and $\partial\boldsymbol{\alpha}^{(2)}/\partial\hat{u}$ at the surface must be 400$\times$ larger than for the bulk LO phonon. A $\sim$20$\times$ enhancement in both tensors may come from the surface atoms not being confined on the vacuum side and the 2D confinement of the surface electronic wave function. Large surface deformation potentials drive dramatic reconstructions on covalent surfaces and enhance cross sections for adsorbate ir and Raman modes. The surface atomic displacement is likely $\sim$0.005 Å. Further susceptibility enhancement may occur because the pump photon energy (1.5 eV) is nearly resonant with the occupied-to-unoccupied dangling bond transition and the SH energy is nearly resonant with the backbonding-to-unoccupied dangling bond transition [16]. Resonant enhancement of Raman scattering from Sb-GaAs (110) interface phonons was observed in the 3–4 eV range [9].

In conclusion, we excited coherent local surface phonons with femtosecond laser pulses. We probed the free induction decay of these phonon modes by time-resolved SHG. The signal/noise and spectral resolution are better than those obtained with HREELS but we detect only modes at $q_{\parallel} \sim 0$. The general nature of the driving mechanisms (SRE or MGR) and of enhanced surface electron-phonon coupling suggests this technique may be used as a general surface vibrational spectroscopy tool. The ability to excite large amplitude coherent surface phonons suggests that we may someday use these phonons to explore nonthermal surface chemistry and to probe phonon-specific phonon-phonon and electron-phonon interactions.

[1] G. C. Cho, W. Kutt, and H. Kurz, Phys. Rev. Lett. **65**, 764 (1990).

[2] W. A. Kutt, W. Albrecht, and H. Kurz, IEEE J. Quantum Electron. **28**, 2434 (1992), and references therein.

[3] T. K. Cheng, S. Vidal, M. J. Zeiger, G. Dresselhaus, M. S. Dresselhaus, and E. P. Ippen, Appl. Phys. Lett. **58**, 980 (1991).

[4] M. J. Zeiger, S. Vidal, T. K. Cheng, E. P. Ippen, G. Dresselhaus, and M. S. Dresselhaus, Phys. Rev. B **45**, 768 (1992).

[5] L. Xu, Y. M. Chang, and H. W. K. Tom, *Ultrafast Phenomena IX* (Springer-Verlag, Berlin, 1994), pp. 333–336.

[6] U. Harten and J. P. Toennies, Europhys. Lett. **4**, 833 (1987); R. B. Doak and D. B. Nguyen, J. Electron Spectrosc. Relat. Phenom. **44**, 205 (1987).

[7] H. Nienhaus and W. Mönch, Phys. Rev. B **50**, 11 750 (1994).

[8] M. Hunermann, J. Geurts, and W. Richter, Phys. Rev. Lett. **66**, 640 (1991).

[9] N. Esser, M. Kopp, P. Haier, A. Kelnberger, and W. Richter, J. Vac. Sci. Technol. B **11**, 1481 (1993).

[10] J. Fritsch, P. Pavone, and U. Schröder, Phys. Rev. Lett. **71**, 4194 (1993).

[11] T. J. Godin, J. P. LaFemina, and C. B. Duke, J. Vac. Sci. Technol. B **9**, 2282 (1991).

[12] R. Matz and H. Lüth, Suppl. Le Vide, Les Couches Minces **201**, 762 (1980); L. H. Dubois and G. P. Schwartz, Phys. Rev. B **26**, 794 (1982).

[13] R. Fuchs and K. L. Kliewer, Phys. Rev. **140**, A2076 (1965).

[14] Y. X. Yan, E. B. Gamble, and K. A. Nelson, J. Chem. Phys. **83**, 5391 (1985).

[15] D. Menzel and R. Gomer, J. Chem. Phys. **41**, 3311 (1964); P. A. Redhead, Can. J. Phys. **42**, 886 (1964).

[16] See Fig. 3 in R. Honke, J. Fritsch, P. Pavone, and U. Schröder, Phys. Rev. B **53**, 9923 (1996).